2018

An Experimentally Validated Model of Single-Phase Flow Distribution in Brazed Plate Heat Exchangers

Wenzhe Li
Air-Conditioning and Refrigeration Center (ACRC), University of Illinois Urbana-Champaign, United States of America, liwz310@illinois.edu

Predrag S. Hrnjak
pega@illinois.edu

Follow this and additional works at: https://docs.lib.purdue.edu/iracc

An experimentally validated model of single-phase flow distribution in brazed plate heat exchangers

Wenzhe LI[1], Pega HRNJAK[1, 2] *

[1] Air-Conditioning and Refrigeration Center (ACRC),
University of Illinois Urbana-Champaign,
Urbana, IL, USA
liwz310@illinois.edu, pega@illinois.edu

[2] Creative Thermal Solutions In. (CTS),
Urbana, IL, USA

* Corresponding Author

ABSTRACT

This paper presents a mathematical model to predict single-phase flow distribution in brazed plate heat exchangers (BPHEs). In this model, the flow distribution among parallel channels is predicted by imposing the condition that each flow path in the heat exchanger has an identical total pressure drop. The model has been validated by the experiments, in which the pressure drop of gas flow in the headers, as well as across the channels is measured. This model is then used to explore the effect of maldistribution on the thermal performance of the heat exchangers.

The experimental and modeling results show that, for a U-type BPHE, the channel mass flow rate generally decreases along the flow direction in the inlet header. The single-phase maldistribution is highly depending on the relative magnitude of the pressure change along the headers and the pressure drop through the plate channels. For given heat transfer area, a heat exchanger with a longer plate would benefit from less non-uniformity in mass and higher heat transfer coefficient, but suffer from higher overall pressure drop.

1. INTRODUCTION

Brazed plate heat exchangers (BPHEs) have been widely used in the heating, ventilating, air conditioning, and refrigeration industry, among many others. But the maldistribution of refrigerant among parallel channels is still one of the main issues. For single-phase flow, the distribution of fluid among parallel channels is basically determined by the header induced pressure drop, as well as the pressure drop cross the channels. The maldistribution would generally decrease the performance of BPHEs by causing higher pressure drop and poor utilization of heat transfer area.

Several researchers have studied on modeling of single-phase flow distribution in plate heat exchangers and similar structures. Bajura and Jones (1976) proposed an analytical model for the dividing and combing manifold system. They identified several factors affecting flow distribution, including the momentum correction factor, which considers the axial momentum transport through the channels and the velocity profile correction factor, which accounts for the non-uniformity of velocity profile in the manifolds. Bassiouny and Martin (1984a, 1984b) developed a one-dimensional mathematical model to analyze single-phase flow distribution and pressure drop for the U-type and Z-type plate heat exchangers. They defined a general characteristic parameter which determines the flow behavior in all heat exchangers. Wang (2011) established a theoretical model for the manifolds distribution system. In his work, both the friction effect and inertial effect in the manifolds have been included. Wang et al. (2011) applied CFD tool to characterize the flow distribution in compact flow heat exchangers. Their results showed that the jet flow induced by the sudden expansion of the header at the entrance has a significant impact on the flow distribution.

The objective of this paper is to present a one-dimensional, discrete mathematical model which describes single-phase flow distribution in BPHEs and use this model to explore the effect of maldistribution on the thermal performance of the heat exchangers.

2. MODEL DESCRIPTION

In this model, the mass flow rate distribution is calculated based on the principle of "identical total pressure drop" for each flow path. In a heat exchanger, a flow path starts from the entrance, passes through the inlet header, a plate channel and the outlet header, and eventually ends at the exit. Based on fluid mechanics, the total pressure drop between the entrance and exit of the heat exchanger should be identical for each flow path. Imposing this condition and correlating the pressure drop with the mass flow rate, the distribution is then solved out. This model computes the total pressure drop by decomposing it into three components: the pressure change along the inlet/outlet headers and the pressure drop across the channel, as shown in Figure 1. The calculation of the pressure drop in these components would be described in following sections.
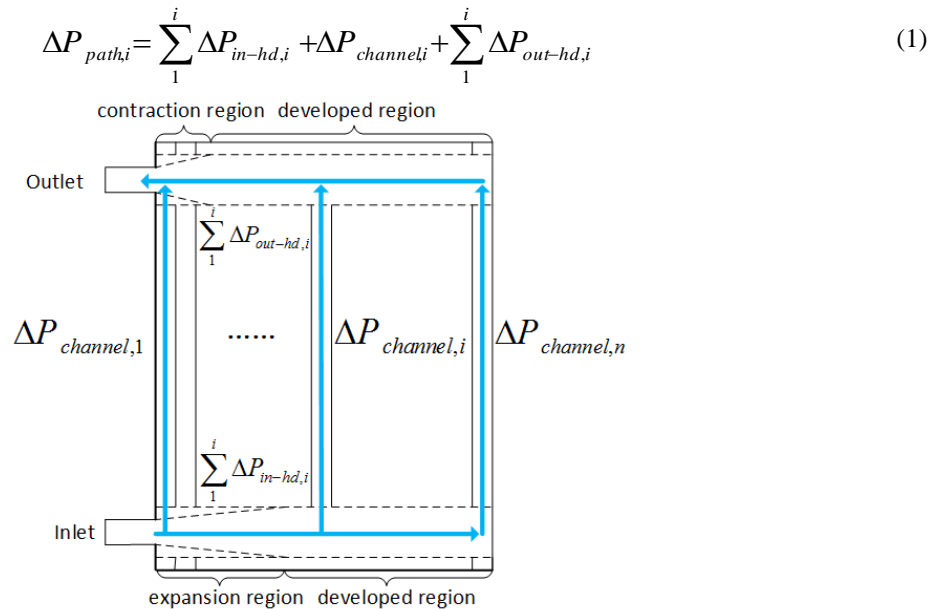
$$\Delta P_{path,i} = \sum_{1}^{i} \Delta P_{in-hd,i} + \Delta P_{channel,i} + \sum_{1}^{i} \Delta P_{out-hd,i} \tag{1}$$

Figure 1: Schematic of the pressure drop calculation

2.1 Pressure drop in the inlet header

Referring to Wang et al. (2011), the jet flow induced by the sudden expansion of the inlet header at the entrance significantly affects the distribution. To address this issue, the inlet header is divided into two regions: the expansion region near the entrance, in which the readjustment of velocity profile happens; the developed region, in which the main stream occupies the entire across section of the inlet header, as shown in Figure 1.

For the developed region, a control volume could be taken at the inlet header corresponding to a plate channel, as shown in Figure 2(a). The mass and momentum conservation equation can be written as following:

$$\rho \bar{v}_{in,i} A = \rho \bar{v}_{in,i+1} A + \rho \bar{u}_{ci} A_c \tag{2}$$

$$P_{in,i} A - P_{in,i+1} A = \beta_{in,i+1} \rho A \bar{v}_{in,i+1}^2 - \beta_{in,i} \rho A \bar{v}_{in,i}^2 + \left(\rho A_c \bar{u}_{ci} \right) \bar{v}_{ci} \tag{3}$$

where β, defined by Equation (4), is the velocity profile correction, which accounts for the non-uniformity of transversal velocity profile:

$$\beta_{in,i} = \frac{\int \rho v_{in,i}^2 dA}{\rho A \bar{v}_{in,i}^2} \tag{4}$$

Generally, β depends on the flow condition and structure of the heat exchanger (Bajura and Jones, 1976). For purposes of simplification, it is taken to be 1.4 based on the previous CFD simulation of the gas flow in the inlet

header (Li and Hrnjak, 2016). The third term in the right-hand side of Equation (3) denotes the axial momentum transported by the channel flow. $\bar{v}_{ci}$, which is the axial velocity component of the fluid entering into the channel, is approximated to be $0.8 \cdot \bar{v}_{in,i}$ according to López et al. (2012). It is also noticeable that the friction effect is not included in the momentum equation. This is because the main stream in the header actually does not touch the metal plate surface; instead it flows through a series of the concentric holes formed by the plates. Combining Equation (2) and (3), the pressure difference between two adjacent control volumes could be obtained:

$$\Delta P_{in-hd,i} = P_{in,i} - P_{in,i+1} \tag{5}$$

For the expansion region, the first task is to determine its length. The flow in the expansion region could be analogized to the flow in an abruptly expanding duct. Many researchers have studied on this topic and concluded that the turbulent reattachment length, which is the distance between separation and reattachment, is about 6~9 step heights (Morrison et al. 1988). Considering the fact that the reattachment would be earlier if the fluid is branching out through the channels, the expansion length in this model is selected to be 6 step heights. To model the readjustment of velocity profile, the diameter of the main stream is assumed to expand linearly from the diameter of the entrance to the diameter of the header over the expansion length. Then, the mass and momentum conservation equation can be written for a control volume in the expansion region, as shown in 2(b):

$$\rho \bar{v}_{in,i} A_i = \rho \bar{v}_{in,i+1} A_{i+1} + \rho \bar{u}_{ci} A_c \tag{6}$$

$$P_{in,i} A - P_{in,i+1} A = \beta_{in,i+1} \rho A_{in,i+1} \bar{v}^2_{in,i+1} - \beta_{in,i} \rho A_{in,i} \bar{v}^2_{in,i} + \left(\rho A_c \bar{u}_{ci} \right) \bar{v}_{ci} \tag{7}$$

The difference between Equation (2), (3) and (6), (7) is replacing a constant main stream cross-sectional area to a variable area. β in Equation (7) is still taken to be 1.4. However, due to the existence of recirculation zone near inlet of the channels, $\bar{v}_{ci}$ should be negative. Here, it is assumed to be $-\bar{v}_{in,i}$.

Similarly, the pressure difference between two adjacent control volumes could be obtained through Equation (6) and (7).
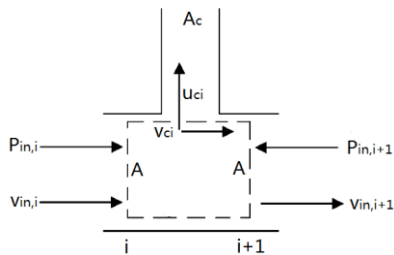

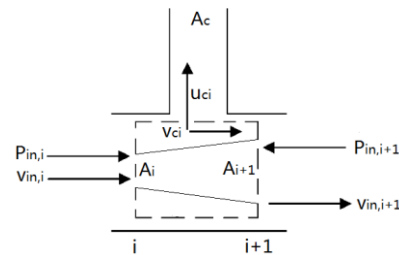**Figure 2(a):** Control volume in the developed region of the inlet header

Figure 2(b): Control volume in the expansion region of the inlet header

2.2 Pressure drop in the outlet header
Similar to the treatment of the inlet header, the outlet header is also divided into two regions: the developed region and the contraction region. For the developed region, the control volume is taken as in Figure 3(a). The mass and momentum conservation equation can be written as following:

$$\rho \bar{v}_{out,i} A = \rho \bar{v}_{out,i+1} A + \rho \bar{u}_{ci} A_c \tag{8}$$

$$P_{out,i} A - P_{out,i+1} A = \beta_{out,i+1} \rho A \bar{v}^2_{out,i+1} - \beta_{out,i} \rho A \bar{v}^2_{out,i} \tag{9}$$

It is worthy noticing that there is no axial momentum transport term in Equation (9). This is because the flow in the channels has been regulated into pure vertical direction and it does not carry any axial momentum when leaving the channels. For the outlet header, β is selected to be 1.33 based on Bajura and Jones (1976). The pressure difference is then calculated for the developed region.

For the contraction region, the determination of its length is based on the studies of flow through the sudden contractions. Khezzar and Whitelaw (1988) concluded that for turbulent flow in the axisymmetric contractions, the major changes in approach velocity profile takes place in a distance of half an upstream diameter. Therefore, the length of the contraction region is assumed to be half a diameter of the header. Similarly, the diameter of the main stream is assumed to contract linearly. The mass and momentum conservation equation for a control volume in this region, shown in Figure 3(b), are given as following:

$$\rho \bar{v}_{out,i} A_i = \rho \bar{v}_{out,i+1} A_{i+1} + \rho \bar{u}_{ci} A_c \tag{10}$$

$$P_{out,i} A - P_{out,i+1} A = \beta_{out,i+1} \rho A_{i+1} \bar{v}_{out,i+1}^2 - \beta_{out,i} \rho A_i \bar{v}_{out,i}^2 \tag{11}$$
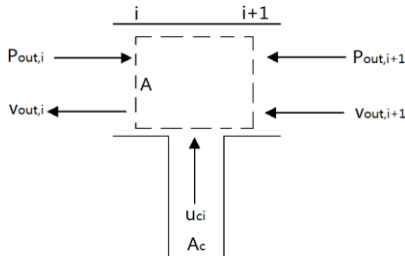
The pressure difference is then calculated accordingly.

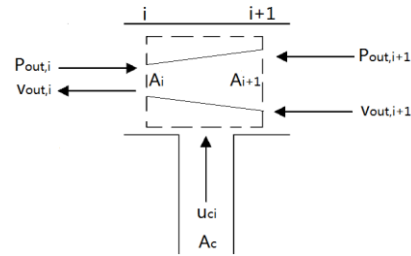**Figure 3(a):** Control volume in the developed region of the outlet header

Figure 3(b): Control volume in the expansion region of the outlet header

2.3 Pressure drop across the channel

The pressure drop across the channel consists of four components: the local pressure loss of entering the channel, the frictional pressure drop, the gravitational pressure drop and the local pressure loss of exiting the channel.

$$\Delta P_{channel} = \Delta P_{entering} + \Delta P_{friction} + \Delta P_{gravity} + \Delta P_{exiting} \tag{12}$$

Among them, the local pressure loss of entering/exiting the channel is calculated based on the correlations in Idel'chick (1994). The frictional and gravitational pressure drop is estimated as following:

$$\Delta P_{friction} = f \frac{\rho u_{ci}^2}{2} \frac{4L_v}{D_h} \tag{13}$$

$$\Delta P_{gravity} = \rho g L_v \tag{14}$$

The friction factor f in Equation (13) is obtained through the gas-phase experiments, which would be discussed in the next section.

2. MODEL VALIDATION

This model has been experimentally validated. In the experiments, the pressure drop of gas flow along the inlet/outlet header, as well as across the channels is measured. The working fluid is nitrogen and the total mass flow rate varies from 10 g/s to 30 g/s. The detailed description of the experimental facility and procedure can be found in Li and Hrnjak (2016). The comparison between the modeling results and experimental data of the pressure change in the headers is given in Figure 4.

In Figure 4, the solid and empty dots denote the experimental data of the inlet and outlet header; the solid and dash lines are the modeling results of the inlet and outlet header. It can be seen in Figure 4, the modeling results agree well with the experimental data. In the inlet header, the static pressure increases along the flow direction. This is because the flow in the inlet header decelerates with the fluid continuously branching out through the channels. Thereby, the dynamic pressure is converted to the static pressure and that gives a pressure rise along the inlet header. In addition, the pressure rise near the entrance is much more rapid than that of the rear part due to existence of the expansion region. The pressure change in the outlet header is opposite to the inlet header. With the fluid continuously entering the outlet header through the channels, the flow in the header accelerates. The static pressure is converted to the dynamic pressure and causes pressure decrease along the outlet header. Similarly, the rapid pressure drop before the exit is caused by the sudden contraction. For the BPHE tested here, the length of the expansion region in the inlet header is longer than that of the contraction region in the outlet header.

Figure 5 shows the modeling results and experimental data for the pressure drop across the channels, which is a direct indicator of the mass flow rate in the channels. It can be seen in Figure 5, along the flow direction in the inlet header, the pressure drop first decreases and then increases for the channels near the entrance/exit of the heat exchanger. This rapid variation of the pressure drop is the result of unequal length between the expansion region and

contraction region of the tested BPHE. For the channels beyond this region, the pressure drop generally decreases with the distance away from the entrance/exit. This could attribute to that the pressure drop in the outlet header is larger than the pressure gain in the inlet header due to the lack of axial momentum transport term in Equation (9).
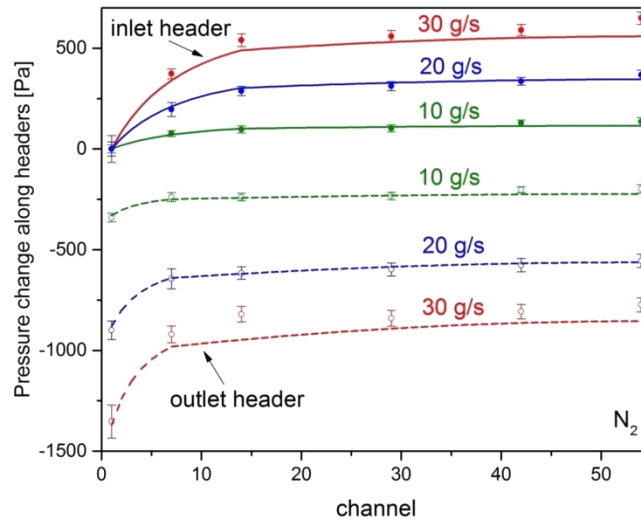
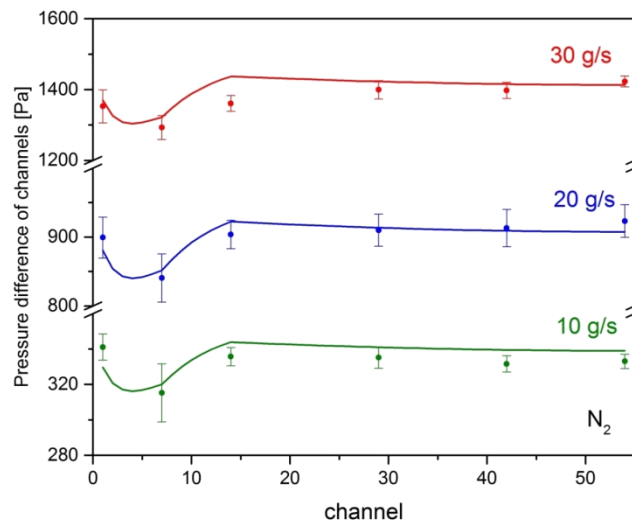**Figure 4:** Modeling vs. experiments: pressure change in the headers

Figure 5: Modeling vs. experiments: pressure drop across the channels

3. PREDICTED EFFECTS OF MALDISTRIBUTION ON THERMAL PERFORMANCE

In above discussion, a single-phase distribution model has been developed and experimentally validated. By using this model, the effect of maldistribution on the thermal performance of the BPHE could be explored. Several assumptions are made to simplify the heat transfer calculation: (1) heat transfer does not affect the single-phase distribution; (2) heat transfer only takes place through plates; (3) for a single plate channel, the thermal properties keep unchanged; (4) the thermal resistance of the plate can be neglected. Based on above assumptions, the heat transfer is computed by following equations:

For the hot side channel:

$$\left(\dot{m}C_p\right)_h\left(T_{h,in,i}-T_{h,out,i}\right)=U_i A \cdot LMTD_i + U_i' A \cdot LMTD_i' \tag{15}$$

For the cold side channel:

$$\left(\dot{m}C_p\right)_c\left(T_{c,out,i}-T_{c,in,i}\right)=U_i A \cdot LMTD_i + U_{i-1}' A \cdot LMTD_{i-1}' \tag{16}$$

where:

$$LMTD_i = \left[\left(T_{h,in,i} - T_{c,out,i}\right) - \left(T_{h,out,i} - T_{c,in,i}\right)\right] \Big/ \ln\left(\frac{T_{h,in,i} - T_{c,out,i}}{T_{h,out,i} - T_{c,in,i}}\right) \tag{17}$$

$$LMTD_i' = \left[\left(T_{h,in,i} - T_{c,out,i+1}\right) - \left(T_{h,out,i} - T_{c,in,i+1}\right)\right] \Big/ \ln\left(\frac{T_{h,in,i} - T_{c,out,i+1}}{T_{h,out,i} - T_{c,in,i+1}}\right) \tag{18}$$

$$U_i^{-1} = h_{h,i}^{-1} + h_{c,i}^{-1} \tag{19}$$

$$U_i^{r-1} = h_{h,i}^{-1} + h_{c,i+1}^{-1} \tag{20}$$

The geometric parameters of the heat exchanger studied are given in Table 1. This heat exchanger is chosen because its single-channel thermal and hydraulic performance has been studied (Jin and Hrnjak, 2017). The friction factor in Equation (13) and the heat transfer coefficients in Equation (19), (20) are obtained based on the correlations in Jin and Hrnjak, 2017. It is also assumed that the size of the entrance/exit of this heat exchanger is the same as the size of the headers. Therefore, the expansion region and contraction regions are excluded when calculating the distribution.

Table 1: Geometric parameters of modeled heat exchanger

Parameter	
Chevron angle, φ, °	60
Corrugation depth, b, mm	2.20
Corrugation pitch, P_c, mm	10.0
Plate thickness, t, mm	0.60
Port length, L_p, mm	495
Total length, L_v, mm	578
Port width, L_h, mm	140
Total width, L_w, mm	210
Heat transfer area, A_{plate}, m^2	0.0900
Port diameter, D_p, mm	35.0

The calculation procedure is: first, by the developed distribution model, the mass flow rate distribution for both hot side and cold side are obtained; then with given distributions, the heat transfer in each channel is iteratively solved by Equation (15) ~ (20). The heat transfer calculation is under the condition: the hot side: water with inlet temperature at 40 °C, the averaged channel mass flow rate $\dot{m}_{channel,avg}$= 30 g/s, flowing upward; the cold side: water with inlet temperature at 20 °C, the averaged channel mass flow rate $\dot{m}_{channel,avg}$= 30 g/s, flowing downward. Three heat exchangers with different number of plates (10, 50, 100 plates) have been modeled.

To quantify the flow maldistribution among channels, the coefficient of distribution, defined by Equation (21), is used. Higher non-uniformity in mass flow rate results in a higher σ.

$$\sigma = \frac{1}{\dot{m}_{channel,avg}} \sqrt{\frac{1}{n}\sum_1^n \left(\dot{m}_i - \dot{m}_{channel,avg}\right)^2} \tag{21}$$

Figure 6(a) shows the calculated pressure profile in the inlet/outlet headers, as well as the predicted mass flow rate distribution in the heat exchanger with 10 plates. It can be seen in Figure 6(a) that the pressure change in the headers is almost negligible and the distribution of mass flow is thereby uniform in this case. The coefficient of distribution is also approximately to be zero in both hot and cold side. It is worthwhile noticing that because the fluid is flowing downward in the hot side and the length of the plate is relatively large, the pressure in the inlet header is actually smaller than that in the outlet header, which gives a negative channel pressure drop in the hot side.

The outlet temperature and heat capacity in each channel of the heat exchanger with 10 plates are given in Figure 6(b).With a uniform mass flow rate distribution in both hot and cold side, the outlet temperature and heat capacity distribution is not uniform. This is because two channels at ends are the cold channels, which only receive heat from

one neighboring hot channel. Thus, they have a low outlet temperature and heat capacity. Two hot channels which neighbor two end channels have a low outlet temperature and a high heat capacity due to a higher temperature difference between them with two end channels. The rest channels generally have almost the same outlet temperature and heat capacity.

Figure 7(a), 7(b) and 8(a), 8(b) give the modeling results for the heat exchanger with 50 and 100 plates respectively. With more plates, the maldistribution becomes more severe and the coefficient of distribution becomes larger. As discuss before, for the U-type heat exchanger, the channels close to the entrance/exit of the heat exchanger would receive more mass flow. This conclusion holds for both hot and cold sides. From Figure 7(a), 8(a), one could see that the pressure drop in headers become more significant as the number of plates and the total mass flow rate increase. This indicates the pressure drop in headers suppresses the pressure drop across the channels and causes a more severe maldistribution. Another thing should be noticed that the magnitude of the channel pressure drop in the cold side is larger than that in the hot side. This is because in the hot side, the gravitational pressure drop is acting opposite to the frictional and local pressure loss in channels. However, this difference in channel pressure drop seems not to affect the mass flow rate distribution in two sides very much. Observed from Figure 7(a), 8(a), the hot side and cold side almost have the same mass flow rate distribution profile and therefore the outlet temperature is relatively constant, except for the channels at two ends. Consequently, the heat capacity distribution generally follows the profiles of the mass flow distribution, as shown in Figure 7(b), 8(b).
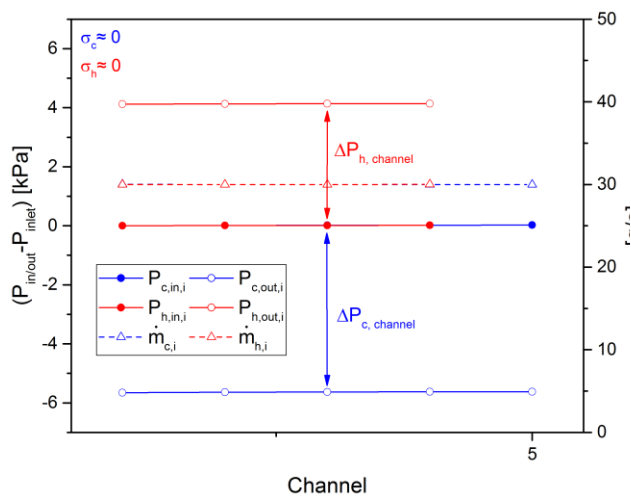

Figure 6(a): Mass flow rate distribution and pressure profile in heat exchanger with 10 plates.
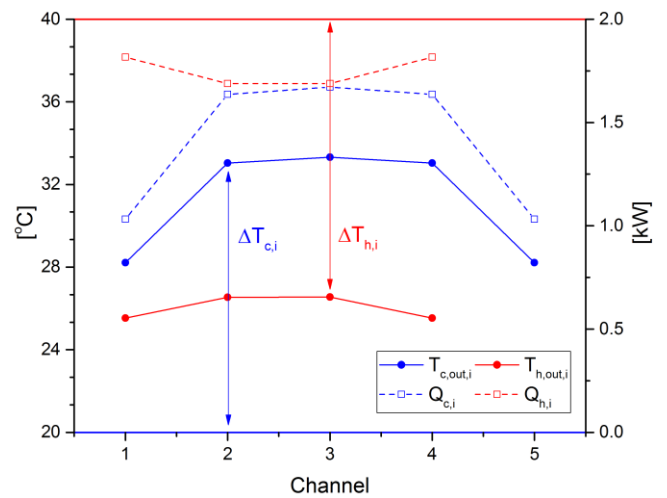

Figure 6(b): Outlet temperature of channels and heat capacity distribution in heat exchanger with 10 plates.
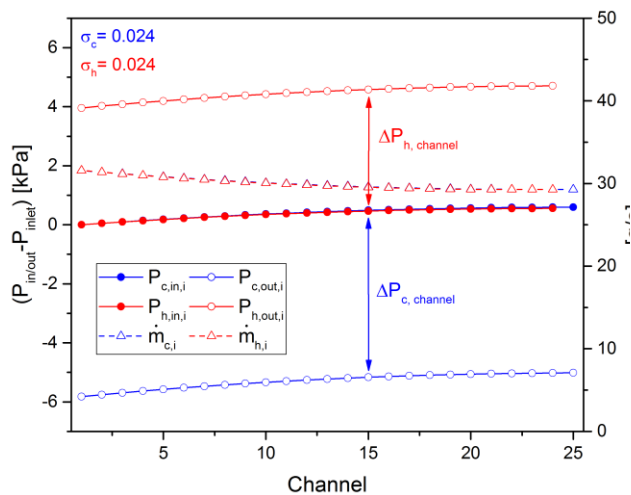

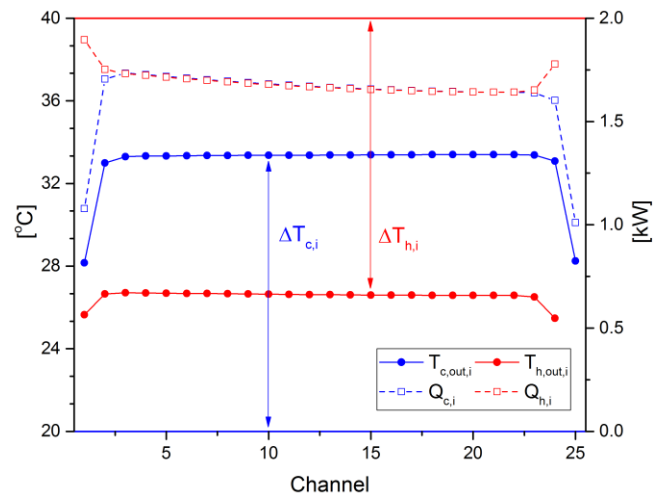**Figure 7(a):** Mass flow rate distribution and pressure profile in heat exchanger with 50 plates.

Figure 7(b): Outlet temperature of channels and heat capacity distribution in heat exchanger with 50 plates.
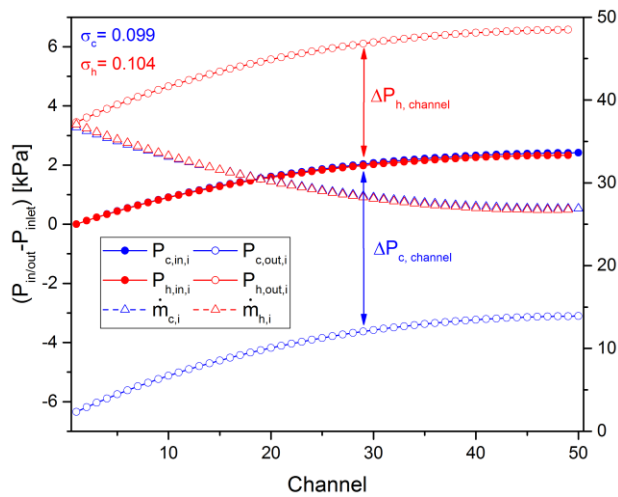
Figure 8(a): Mass flow rate distribution and pressure profile in heat exchanger with 100 plates.
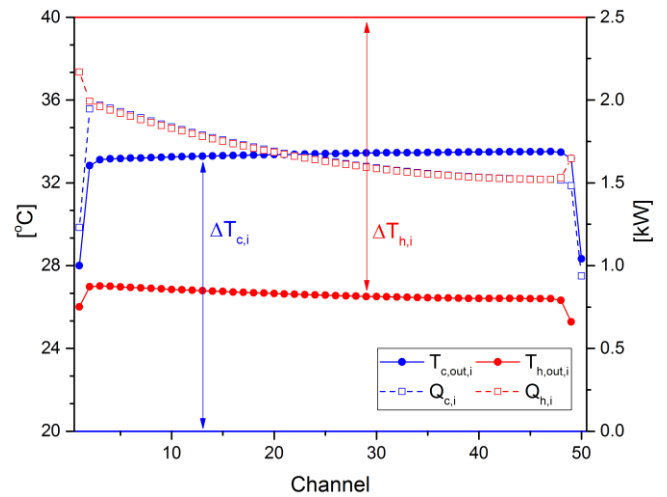

Figure 8(b): Outlet temperature of channels and heat capacity distribution in heat exchanger with 100 plates

As mentioned before, the header induced pressure drop is one of the main causes of fluid maldistribution and the relative magnitude of the pressure drop in headers and in channels would significantly affect the distribution. To further explore this issue, the heat exchangers with varying length of the plate (100 %, 75 %, and 50 % of the original length) have also been modeled and compared. To make the cases comparable, the width of the plate is accordingly changed with varying length of the plate to keep the heat transfer area unchanged. The results are given in Figure 9 and Figure 10.

Figure 9 shows the mass flow rate distribution in the heat exchangers with varying plate length. It is obvious that the maldistribution becomes severe when reducing the plate length. This is because the pressure drop in channels would be reduced with a shorter plate and that makes the header induced pressure drop dominant in the overall pressure drop. Figure 10 compares the total heat capacity and pressure drop in the heat exchangers. According to Figure 10, the total heat capacity would be reduced when the length of the plate reduced, even if the total heat transfer area is maintained. This is mainly caused by the reduction of heat transfer coefficient, which is the result of expanded width of channels. With a smaller plate length, the overall pressure drop across the heat exchanger is decreased, as shown in Figure 10. The results in Figure 9 and Figure 10 indicate that with given heat transfer area, a heat exchanger with a longer plate would benefit from less non-uniformity in mass and higher heat transfer coefficient, but suffer from a higher overall pressure drop.
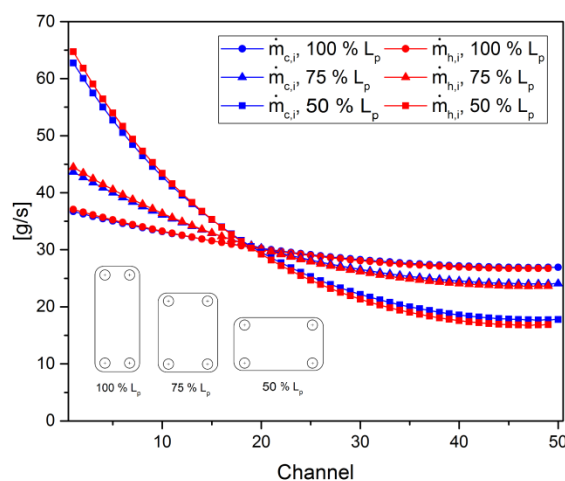

Figure 10(a): Mass flow rate distribution in heat exchanger with 100 plates, varying length of the plate.
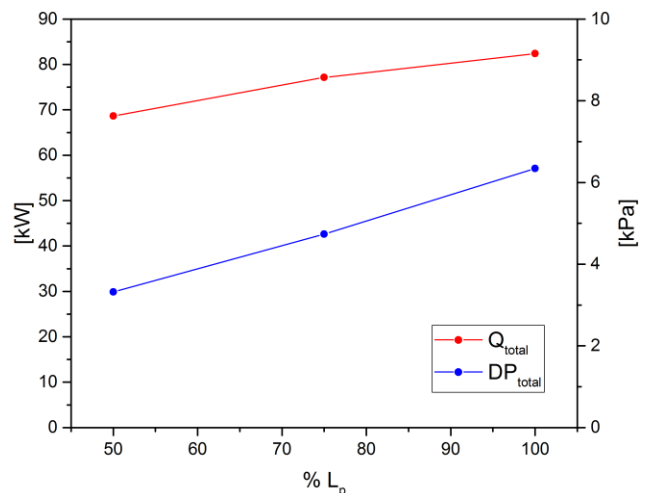

Figure 10(b): Reducing the length of the plate reduces the heat capacity and pressure drop.

4. SUMMARY AND CONCLUSION

This paper presents a one-dimensional, discrete model for single-phase flow distribution in BPHEs based on the principle of "identical total pressure drop" for each flow path. This model has been validated by the measurements of the gas flow pressure drop. The developed model is then used to explore the effects of maldistribution on thermal performance of the heat exchanger. The calculation results show that the single-phase maldistribution is highly depending on the relative magnitude of the pressure change along the headers and the pressure drop through the plate channels. For given heat transfer area, a heat exchanger with a longer plate would benefit from less non-uniformity in mass and higher heat transfer coefficient, but suffer from higher overall pressure drop.

NOMENCLATURE

A	Area	m^2
C_p	Specific heat	$J\ kg^{-1}\ {}^oC^{-1}$
D_h	Hydraulic diameter	m
F	Friction factor	-
g	Gravitational acceleration	$m\ s^{-2}$
h	Heat transfer coefficient	$W\ m^{-2}\ {}^oC^{-1}$
L	Length	m
$\dot{m}$	Mass flow rate	$kg\ s^{-1}$
P	Pressure	Pa
T	Temperature	^oC
u	Velocity in channel	$m\ s^{-1}$
U	Overall heat transfer coeff.	$W\ m^{-2}\ {}^oC^{-1}$
v	Velocity in headers	$m\ s^{-1}$

Greek Symbols

β	Velocity profile correction	-
ρ	Density	$kg\ m^{-3}$
σ	Coeff. of distribution	-

Subscript

avg	Average
c	Cold, or channel
h	Hot
in	Inlet
out	Outlet

REFERENCES

Bajura, R. A., Jones, Jr E. H. (1976). Flow distribution manifolds. *J. Fluids Eng. Trans. ASME*, 98,654-665.

Bassiouny, M. K., Martin, H. (1984a). Flow distribution and pressure drop in plate heat exchangers-I: U-type arrangement. *Chemical Engineering Science*, 39(4), 693-700.

Bassiouny, M. K., Martin, H. (1984b). Flow distribution and pressure drop in plate heat exchangers-II: Z-type arrangement. *Chemical Engineering Science*, 39(4), 701-704.

Idel'chik, I. E., (1994). Handbook of hydraulic resistance, CRC Press.

Jin S., Hrnjak, P. (2017). Effect of end plates on heat transfer of plate heat exchanger, *International Journal of Heat and Mass Transfer,*108(Part A), 780-784.

Khezzar, L., Whitelaw, J. H. (1988). Flows through round sudden contractions, *Proc. Instn. Mech. Engrs.*, 202(C4), 295-300.

Li, W., Hrnjak, P. (2016). Single phase pressure drop and flow distribution in brazed plate heat exchangers. *International Refrigeration and Air Conditioning Conference*, Paper 1812.

López, R., Lecuona, A., Ventas, R., & Vereda, C. (2012). A numerical procedure for flow distribution and pressure drops for U and Z type configurations plate heat exchangers with variable coefficients. *Journal of Physics: Conference Series*, Volume 395, conference 1.

Morrison, G. L., Tatterson, G. B. & Long, M. W. (1988). Three-dimensional laser velocimeter investigation of turbulent, incompressible flow in an axisymmetric sudden expansion. *Journal of Propulsion and Power*, 4(6), 533-540.

Wang, C. C., Yang, K. S., Tsai, J. S. & Chen, I. Y. (2011). Characteristics of flow distribution in compact parallel flow heat exchangers, part I: typical inlet header, *Applied Thermal Engineering*, 31, 3226-3234.

Wang, J. (2011). Theory of flow distribution in manifolds, *Chemical Engineering Journal*, 68, 1331-1345.

ACKNOWLEDGEMENT